Catalysis Today xxx (xxxx) xxx–xxx

Contents lists available at ScienceDirect

Catalysis Today

journal homepage: www.elsevier.com/locate/cattod

Ozone initiated oxidation of 1,2-dichlorobenzene catalyzed by manganese loaded gamma alumina and silica

Nomthandazo Mkhize[a], Prabal Pratap Singh[b], Deepak Kumar Das[b], Viswanadha Srirama Rajasekhar Pullabhotla[a,*]

[a] Department of Chemistry, University of Zululand, Private Bag X1001, Kwa-Dlangezwa, 3886, South Africa
[b] Department of Chemistry, GLA University, Mathura, UP, 281406, India

ARTICLE INFO

Keywords:
Oxidation
1,2-Dichlorobenzene
$Mn/\gamma\text{-}Al_2O_3$ and Mn/SiO_2 catalysts
Ozone and Mucochloric acid

ABSTRACT

The ozone-initiated oxidation of 1,2-dichlorobenzene catalysed by manganese supported on metal oxide ($\gamma\text{-}Al_2O_3$ and SiO_2) at ambient temperature and pressure conditions is reported in this study. Wet impregnation method was used to synthesise various percentages of Mn loading on $\gamma\text{-}Al_2O_3$ and SiO_2 supports. The catalysts were characterised by FT-IR, SEM, EDX, TEM, ICP-OES, BET and XRD techniques. All the reactions were conducted in an impinger glass reactor using 25 mL pure 1,2-dichlorobenzene and 0.25 g of the catalysts. The reaction products were characterised by GC–MS and FT-IR for quantitative and qualitative identification of the products. The 2.5, 5, 7.5 and 10 % of Mn impregnated on $\gamma\text{-}Al_2O_3$ and SiO_2 were found to be more active than $\gamma\text{-}Al_2O_3$ and SiO_2 supports. The 5 % Mn/SiO_2 catalyst was found to be the most active catalyst in the ozonation reaction of 1,2-dichlorobenzene with a percentage conversion of 44 % and percentage selectivity of 88 % towards the main product mucochloric acid. Whereas, 5 % $Mn/\gamma\text{-}Al_2O_3$ catalyst resulted in the percentage conversion of 40 % and percentage selectivity of 86 % towards the main product mucochloric acid. The activity of the catalysts is attributed to manganese loaded on $\gamma\text{-}Al_2O_3$ and SiO_2 supports.

1. Introduction

There is an increase in global pollution and some of the factors that causes the increase are large number of organic impurities and pollutants that are found in the biosphere, particularly chlorine-based pollutants which are widely known for their non-degradable nature and their high toxicity [1,2]. There are many types of chlorinated organic compounds that are found in the environment, but a certain class of chlorinated organic compounds have received much attention than others due to their bioaccumulation in living tissues and their high toxicity, this class of organic compounds is known as polychlorinated aromatics (PCAs). PCAs have high persistence in the environment which make them immune to degradation by biological processes [3]. These organic compounds are allowed as commercial compounds due to their wide range of applications in agricultural and industrial sectors [4].

Due to the high risk of exposure, the laboratory studies of such compounds are usually undertaken using model compounds, the model compounds include chlorophenols and chlorobenzenes. The model compounds are used to predict the destruction of polychlorinated aromatics under different degradation methods [5]. The common characteristics of the model compounds and PCAs are their chemical behavior and structural properties. In the present study 1,2-dichlorobenzene is used as a model compound so as to predict degradation of PCAs. Since orthodichlororbenzene is also non-biodegradable, its continuous and excessive use as an insecticide is hazardous to environment [6]. This has prompted the researchers to work towards the development of the degradation methods that can be used to convert 1,2-dichlorobenzene into less toxic value-added products [7].

Chlorination process is one of the processes that have been used to inactivate pathogenic microorganism that are found in aqueous environment but it has a disadvantage of initiating the development of by-products that are less oxidizable and more poisonous than the parent material [8]. The studies show that there is a need for process of breaking down organic compounds that is more preferable than chlorination; the process is called ozonation [9,10]. Ozonation is increasingly becoming the important last treatment innovation that is used to improve the removal of color and furthermore the disposal of persevering toxins that are available in the bio-treated effluents [11]. The advantage of ozonation process over chlorination is that it does not

* Corresponding author.
E-mail address: PullabhotlaV@unizulu.ac.za (V.S.R. Pullabhotla).

https://doi.org/10.1016/j.cattod.2020.06.025
Received 4 March 2020; Received in revised form 27 May 2020; Accepted 5 June 2020

require some additional processes in order to remove excess disinfectant from water but higher doses of ozone can be used [12].

Ozone is a powerful oxidant that has been increasingly drawing attention as an alternative oxidant because of its strong capability to degrade hydrocarbons even at low temperature [13,14]. Ozonation reaction involves the direct molecular reactions of ozone with the compounds dissolved and involves the transformation of ozone into secondary oxidants like hydroperoxyl radicals and hydroxyl radicals [11]. Ozonation alone lead to partial mineralization, contrast to this catalytic ozonation can be used due to its higher effectiveness in the degradation of organics [15,16]. Catalytic ozonation is divided into homogeneous catalytic ozonation and heterogeneous catalytic ozonation [17]. In homogenous catalytic ozonation, the decomposition of molecular ozone is catalyzed by the transition metal ions and this process has disadvantages, for example, it results in reaction products that are very hard to separate and the process is less active [16].

In heterogeneous catalytic ozonation, ozone decomposition is catalyzed by metals on metal oxides as supports or metal oxides. In recent years, heterogeneous catalytic process has been receiving an increasing attention because of its high potential effectiveness in the oxidation as well as in the mineralization of stubborn organic pollutants [18]. There are various metal oxide catalysts that have been used in the heterogeneous catalytic ozonation and now they are developed because of their catalytic durability as well as their catalytic performance [19]. Among the catalysts that have been used, alumina has been successfully used in the ozonation of pollutants. Thus V_2O_5/Al_2O_3, V_2O_5/SiO_2, V_2O_5/TiO_2, $CuCO_3/Fe_2O_3$ and so on. Vanadium loaded on titania that is prepared by using sol-gel method showed selectivity and stability that are very high for oxidation of orthodichlorobenzene but vanadium oxide was toxic, however it leads to the formation of secondary pollution [20].

The oxidation reactions where V_2O_5/Al_2O_3, V_2O_5/SiO_2, V_2O_5/TiO_2 were used as catalysts showed high selectivity (98 %–100 %) but little mineralisation [8]. There is no study that has shown the use of manganese loaded on alumina and silica support as catalysts for the oxidation of orthodichlorobenzene. Manganese has a facile redox behavior which facilitates the diffusing of oxygen and high adsorption capacity of oxygen [21]. The main reasons for the wide usage of gamma alumina in many applications as an adsorbent and as a catalyst are its mechanical strength, acid-base properties, thermal stability and high surface area [22]. Silica has also gained a considerable interest due to it high thermal, mechanical and chemical stability, controlled surface area properties and its ability to maintain the dispersion of metals during the reaction [23].

The current study focuses on ozone-initiated oxidation of orthodichlorobenzene catalyzed by manganese loaded on alumina and silica supports at ambient reaction conditions.

2. Materials and methods

2.1. Materials

Aluminium oxide (γ-Al_2O_3, Aldrich, nanopowder < 50 nm particle size, St. Louis, MO, Germany), 1,2-dichlorobenzene (Sigma Aldrich, 99.0 %), manganese(II) chloride tetrahydrate ($MnCl_2{\cdot}4H_2O$, 99.0 %, reagent grade, Aldrich St. Louis, MO, Germany) and silica gel (SiO_2, Merck, 70–230 mesh ASTM). These materials were purchased and used without any further purification.

2.1.1. Catalyst preparation

Wet impregnation method was used to prepare metal (Mn) doped metal oxide catalysts (Mn/γ-Al_2O_3 and Mn/SiO_2). Adequate amount(s) of manganese chloride tetrahydrate that was dissolved in 100 mL of distilled water which was then calculated based on the percentage of manganese (2.5, 5.0, 7.5 and 10.0 Wt%) that was supported on gamma alumina and silica. For example, in this method to prepare 10 g of the 2.5 % Mn loaded on γ-Al_2O_3 (2.5 % Mn/γ-Al_2O_3) catalyst, 0.9025 g of manganese chloride tetrahydrate ($MnCl_2.4H_2O$) was dissolved in 100 mL of distilled water. The prepared solution was slowly dispensed into a 250 mL beaker containing 9.098 g of γ-Al_2O_3 (and beaker containing SiO_2) with vigorous stirring for homogeneous dispersion of Mn onto γ-Al_2O_3 and SiO_2 supports. This was then followed by evaporation of water by placing the beaker on a hot plate at 70 °C until thick paste is obtained and thereafter, this step was completed by drying the catalyst precursor overnight in an oven at 90 °C. The as-synthesized 2.5 % Mn/γ-Al_2O_3 and 2.5 % Mn/SiO_2 catalysts were calcined at 300 °C for 5 h [24]. The similar procedure was followed by using adequate amounts of the $MnCl_2.4H_2O$ to synthesize the 5.0, 7.5 and 10.0 Wt% Mn/γ-Al_2O_3 and Mn/SiO_2 catalysts.

2.1.2. Oxidation of 1,2-dihlorobenzene

The oxidation of 1,2-dichlobenzene was carried out in an impinger unit with porous bubbler of porosity 2. Orthodichlorobenzene was added into the impinger before ozone is fed. Ozone was fed into the impinger unit via a porous bubbler. Initially blank ozonation of 1,2-dichlorobenzene was studied, where ozonation reaction was studied in the absence of the catalyst. Then ozonation reactions was then catalyzed with bare gamma alumina, silica and various percentages of manganese loaded on gamma alumina and silica supports. In all the oxidation reactions 25 mL of 1,2-dichlorobenzene and 0.25 g of catalysts were used.

2.2. Characterisation of catalysts

2.2.1. X-ray diffraction

X-ray diffraction is one the analysis that was performed to characterise the catalysts. This technique was conducted to determine the different phases of Mn (metal) and metal oxide (γ-Al_2O_3 and SiO_2) that is present in the catalyst and also crystal lattice of the support (γ-Al_2O_3 and SiO_2). The powder diffraction patterns were recorded by using a Bruker AXS-D8 with a Cuk_α as radiation source of wavelength 0.15406 nm. Scan speed was 0.2/min over $10-90^\circ$ scan range with operating conditions of 40 kV and 40 mA.

2.2.2. Fourier transform-infrared spectroscopy (FT-IR)

In all calcined catalysts, the functional groups present were identified using FT-IR spectroscopy. The FT-IR spectroscopy analysis was carried out using a Bruker Tensor 27 FT-IR spectrometer with a standard ATR cell. Acetone was used to clean the crystal's surface prior to every analysis. The force gauge adjusted to 22 gauge for proper contact between the surfaces. The mid-IR region for catalyst was kept at the range of $500-4000\ cm^{-1}$.

2.2.3. Scanning Electron Microscope (SEM)

Scanning Electron Microscope was used to study the morphology and topography of the both support and metal loaded calcined catalysts. Carl Zeiss FE-SEM Sigma VP-03-67 instrument was used with operating conditions of 20 kV over a working distance of 6 − 9 mm. All the catalysts samples were dried and ground to fine powder with mortar and pestle prior to the analysis. The analysis was then completed by placing a small amount of the powdered sample on a piece of a two-way carbon tape and then mounted on a stub (sample holder). The compositional analysis of the sample was then carried out on an Oxford instrument X-MaxN 50 mode 54-XMX1003 EXD analyzer.

2.2.4. Transmission Electron Microscopy (TEM)

Transmission electron microscopy was used to study the morphology, particle size and size distribution of all calcined catalysts. The analysis was carried out on a JOEL JEM-2010 electron microscope with an accelerating voltage of 200 kV. The images were captured with Gatan camera and analyzed with Gatan imaging software. The samples were prepared by dispensing fine powder of catalyst in toluene and

sonication for 20 min. Then the drop of a catalyst sample was placed on a holy carbon coated copper grid with mesh size of 150 and allowed to dry at room temperature before TEM images were captured.

2.2.5. Inductively coupled plasma- optical emission spectroscopy (ICP-OES)

The metal content (Mn) of the catalyst was determined using an Agilent 700 series ICP-OES with a 710 ICP-OES detector instrument. A series of standard solutions 25, 50, 75, and 100 ppm were prepared from manganese salt ($MnCl_2.4H_2O$) by dilution with distilled water. The sample preparation was done by digestion of 0.15 g of 2.5, 5.0, 7.5 and 10.0 % Mn loaded catalysts in the mixture of 4 mL HF, 3 mL HCl and 3 mL HNO_3 at 60 °C and then heated until digestion was complete. The resultant solution was diluted with distilled water and made upto 100 mL solutions of 2.5, 5.0, 7.5 and 10.0 % Mn loaded on γ-Al_2O_3 and SiO_2 catalysts.

2.2.6. Brunauer-Emmet-Teller (BET)

BET surface analyser was used to determine the surface areas of as-synthesised catalyst samples. Firstly, the samples were degassed at 250 °C overnight under N_2 flow in micrometrics flow prep 060 as a form of pretreatment. Then the samples were analyzed in an automated and multiple-point micrometrics Gemini 2360 BET surface area under liquid nitrogen conditions.

2.3. Characterization of ozonation reaction product

2.3.1. Fourier transform-infrared spectroscopy (FT-IR)

The FT-IR spectroscopy, as discussed in Section 2.2.2 for the functional group identification of catalysts, was also used to identify functional groups present in the reaction product.

2.3.2. Gas chromatography–mass spectrometry (GC–MS)

GC analysis was carried out on an Agilent 7890A GC system coupled with 5975Vl (Triple axis) Mass Selective Detector (MSD). The column type fitted was an Agilent Hp-5MS, 5 % phenyl methyl siloxane with column dimensions of 30 m x 250µm × 0.25µm. The carrier gas that was used at a flow rate of 0.7 mL/min is helium. The detector temperature and the injection source temperature were 230 and 250 °C respectively. The initial oven temperature was held constant for 2 min then ramped-up to the final temperature of 300 °C at a rate of 6 °C/min. A 6 µL sample was injected with the split ratio 100:1.

3. Results and discussion

3.1. Catalyst characterization results

3.1.1. X-Ray diffraction (XRD)

Fig. 1a shows X-ray diffractograms of γ-Al_2O_3 support and various loading of % Mn/γ-Al_2O_3 catalysts. The XRD peaks that are observed at 2-theta = 33.5°, 37°, 39.8°, 46.9°, 62.2° and 67° are assigned to γ-Al_2O_3 belonging to these hkl values (220), (311), (222), (400), (500) and (440), respectively, with cubic crystal structure (JCPDS 00-010-0425) [25]. There were no diffraction peaks that distinguished the metal or their metal oxide that were detectable for 2.5–7.5 % wt loading of manganese. However, at 10 % Mn/ γ-Al_2O_3 there are two peaks that are observed at 2-theta = 17.5° (101) and 23.2° (111) which can be assigned to tetragonal hausmsnnite Mn_3O_4 (JCPDS No. 24-0734) and pure orthorhombic phase of cubic Mn_2O_3 (JCPDS No. 65-7467) respectively [26]. The X-ray diffractogram shows a decrease in the stability of crystalline of γ-Al_2O_3 as manganese is incorporated into γ-Al_2O_3. This is observed by broadening of the peaks and decrease in the intensity of the peaks as shown in Fig. 1a.

Fig. 1b shows the X-ray diffractograms of SiO_2 support and various % Mn/SiO_2 catalysts. Calcination at 300 °C causes the diffraction peaks to be sharper, as a result the heat treatment at this temperature made gradual crystallization of the material [27]. The X-ray diffractogram

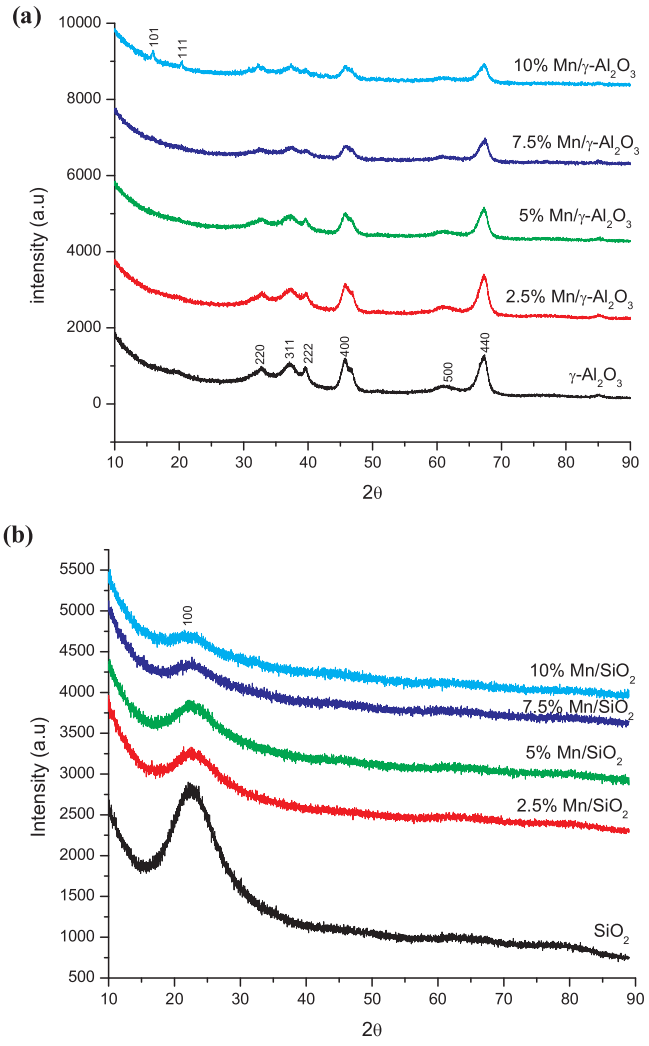

Fig. 1. XRD patterns of (a) γ-Al_2O_3 support, 2.5 % Mn/γ-Al_2O_3, 5 % Mn/γ-Al_2O_3; 7.5 % Mn/γ-Al_2O_3 and 10 % Mn/γ-Al_2O_3 catalysts and (b) SiO_2 support, 2.5 % Mn/SiO_2, 5 % Mn/SiO_2, 7.5 % Mn/ SiO_2 and 10 % Mn/SiO_2 catalysts.

does show a well-defined peak showing amorphous nature of silica. The literature reveals that x-ray diffractograms of metals or metal oxide catalyst containing silica mostly shows only one strong broad peak which is the silica peak thus it the characteristic amorphous nature of silica [28]. Silica support and various percentages of manganese loaded on silica catalysts shows only intense peak at 2-theta = 22.6° (100) which is the peak that is assigned to silica.

3.1.2. Fourier Transform-infrared Spectroscopy (FT-IR)

Fig. 2a shows the FT-IR spectra of various % Mn/γ-Al_2O_3 catalysts and γ-Al_2O_3 support. At around 3450 cm^{-1} there is broad adsorption band which can be ascribed to the vibrational stretching frequency of hydroxyl groups that are present on Lewis acid sites of gamma alumina. These hydroxyl groups result from the dissociative chemisorption of water to Lewis acids sites and also modification of surface of aluminium coordination by protonation of Lewis basic sites [29]. As the percentage of the manganese loaded on gamma alumina increases, these bands are significantly observed. At 1095 cm^{-1} there is a shoulder that is representing Al-O bond. The inter-vibrational mode frequency was observed in the FT-IR spectrum of gamma alumina support and the absorption shoulder within the β range between $950-500\ cm^{-1}$, it is assigned to the octahedral AlO_6 and tetrahedral AlO_4 that are known to reflect at infrared spectrum of gamma alumina [30].

Fig. 2b displays the FT-IR analysis results of SiO_2 and Mn loaded

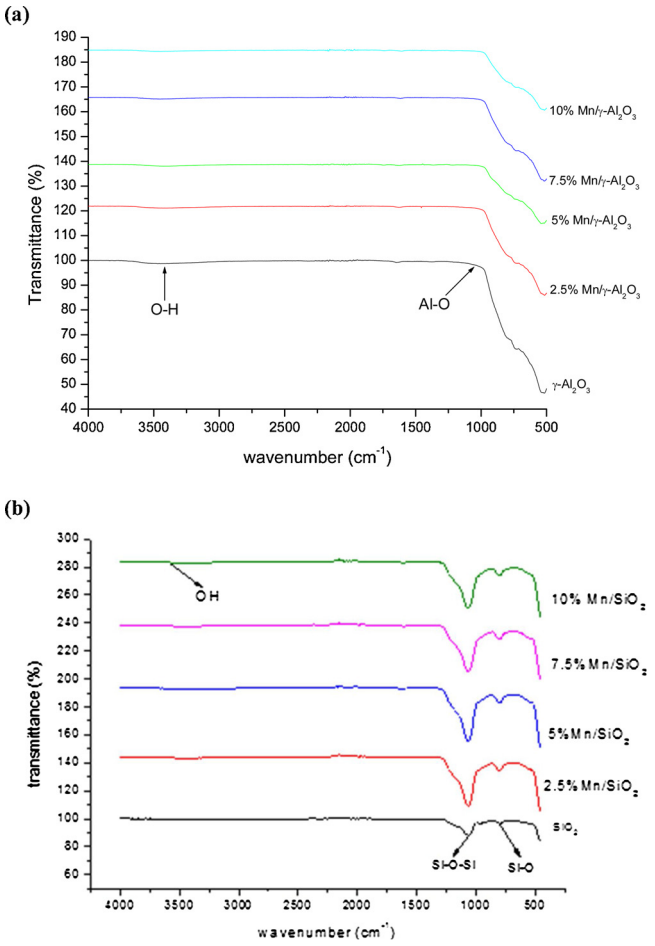

Fig. 2. FT-IR spectra of (a) γ-Al_2O_3 support, 2.5 % Mn/γ-Al_2O_3, 5 % Mn/γ-Al_2O_3, 7.5 % Mn/γ-Al_2O_3 and 10 % Mn/γ-Al_2O_3 catalysts and (b) SiO_2 support, 2.5 % Mn/ SiO_2, 5 % Mn/ SiO_2, 7.5 % Mn/ SiO_2 and 10 % Mn/ SiO_2 catalysts.

SiO_2 catalysts. The spectrum of silica was observed to entail the absorption peaks at 1100 cm^{-1} and 790 cm^{-1}, which corresponds to the stretching of Si-O-Si and bending vibrations of Si-O respectively. The Mn loaded silica catalysts at 2.5 % loading, attained the similar infrared spectra to that of pure silica support. The vibrational stretching frequency of hydrogen atom in hydroxide catalyst appeared at 3445 cm^{-1} for 5 %–10 % nickel loaded on silica [31,32].

3.1.3. Scanning Electron Microscope (SEM)

Fig. 3 below shows the SEM images of γ-Al_2O_3 support and various percentages of Mn loaded γ-Al_2O_3 catalysts. γ-Al_2O_3 support shows the porous nature which appear as fluffy particles with poorly defined structure. The morphology of γ-Al_2O_3 show a rough surface with high surface kinks and defects which belong to metal attached to the support. The surface of gamma alumina becomes fine and aggregated as the Mn content increases. The existence of manganese on γ-Al_2O_3 was further confirmed by EDX images shown in Fig. S1(a–d).

Fig. 4 shows SEM images of SiO_2 support and various percentages of Mn loaded on SiO_2 catalysts. Silica support shows the existence of small black spot that correspond to the pore spaces like cylindrical holes. Silica support is a very fine gel compound aggregate that is surrounded by great number of pores that give the impression of a sponge. Its wide porous texture is said to have well adsorption capacity. At % Mn/SiO_2 catalysts there are small traces of manganese (large white spots) that are distributed on the surface of the catalyst. The existence of manganese on SiO_2 was further confirmed by EDX images shown in Fig. S2(a–d). Figs. S3 and S4 shows the SEM EDX images of 5 % Mn/γ-Al_2O_3 and 5 % Mn/SiO_2 catalysts, these results also suggest that the manganese metal is evenly distributed on the surface of γ-Al_2O_3 and SiO_2 supports.

3.1.4. Transmission Electron Microscopy (TEM)

Fig. 5(a–d) display the TEM images of γ-Al_2O_3 support and various % of Mn loaded γ-Al_2O_3 catalysts. γ-Al_2O_3 shows spherical shape but some of the particles are rod shaped (γ-Al_2O_3 is more spherical shaped than rod shaped) with a particle size ranging from 11 to 15 nm. However, after doping manganese on the γ-Al_2O_3 support rod shaped particles are obtained with varying particle size. The measured average particle size for 2.5 % Mn/γ-Al_2O_3 has a range of 37–63 nm while that of 5 %, 7.5 % and 10 % Mn/γ-Al_2O_3 (Fig. S5) differed only slightly with a particle size range of 30–63 nm, 13–16 nm, and 13–60 nm respectively.

Fig. 6(a–d) shows the TEM images of SiO_2 support and various % of Mn loaded SiO_2 catalysts. SiO_2 has a narrow size distribution (particle size ranging from 19 to 35 nm) with a spherical shape. However, after doping manganese on the SiO_2 support the spherical shape of silica is maintained but when 7.5 % and 10 % Mn/SiO_2 the images show that some of the particles present are rod shaped. The measured average particle size for 2.5 % Mn/SiO_2 has a narrow range of 21–38 nm while that of 5 %, 7.5 % and 10 % Mn/SiO_2 (Fig. S6) differed only slightly with a particle size range of 8–16 nm, 18 −64 nm and 15–75 nm respectively.

3.1.5. Inductively coupled plasma- optical emission spectroscopy (ICP-OES)

Table 1 below show the percentage weight of manganese on each of the Mn/γ-Al_2O_3 which were analyzed using ICP-OES and EDX (Fig. S1 (a–d)). The experimental Mn wt% are close to anticipated theoretical percentages from the results obtained from both ICP and EDX, which suggests that manganese was incorporated successfully onto the surface of gamma alumina.

Table 2 below shows the percentage weight of manganese on each of the Mn/SiO_2 which were analyzed using ICP-OES and EDX. The results from ICP show that actual Mn wt% for the Mn/SiO_2 catalysts is much less than the theoretically calculated wt% for all the catalysts while EDX (Fig. S2 (a–d)) results shows closer values of Mn actual wt% to the theoretically calculated values for 2,5, 5.0 and 7.5 % Mn/SiO_2 catalysts.

ICP-OES data can be affected by spectral interferences which is characterized by an overlap of the analyte (metal loaded metal oxide catalyst) by an interfering element. The background signal for determination of analyte signal can also be interfered. These interferences can result in enhancement/suppression of signals and this can lead to negative or positive results which ultimately lower the accuracy and precision of the method. The reduction of manganese content in ICP-OES data maybe due to uneven dispersion of manganese over the metal oxide supports (γ-Al_2O_3 and SiO_2) and also by significant aggregation of manganese, which can be supported by the SEM-EDX data.

3.1.6. Brunauer-Emmet-Teller (BET)

Table 3 displays the BET results of pure γ-Al_2O_3 support, 2.5 % Mn/γ-Al_2O_3 and 7.5 % Mn/γ-Al_2O_3 catalysts. The BET surface area of γ-Al_2O_3 was found to be 295.0 m^2/g. However, the surface area tends to decrease with metal loading, the BET surface areas of 2.5 % Mn/γ-Al_2O_3 and 7.5 % Mn/γ-Al_2O_3 were found to be 167.6 m^2/g and 107.8 m^2/g respectively confirming the gradual filling of the pore volume of the γ-Al_2O_3 support. Furthermore, the pore volumes of 2.5 % Mn/γ-Al_2O_3 and 7.5 % Mn/γ-Al_2O_3 catalysts were found to be 0.3826 and 0.3022 cm^3/g respectively attributing the incorporation of the Mn into the pore volume of the γ-Al_2O_3 support. The BET results showed the Mn loading into γ-Al_2O_3 support results in decrease of both pore volume and surface area. However, the increase in pore size as surface area decreases was observed. This is caused by pores that are filled and also blocked by manganese particles, which increased the surface of Mn

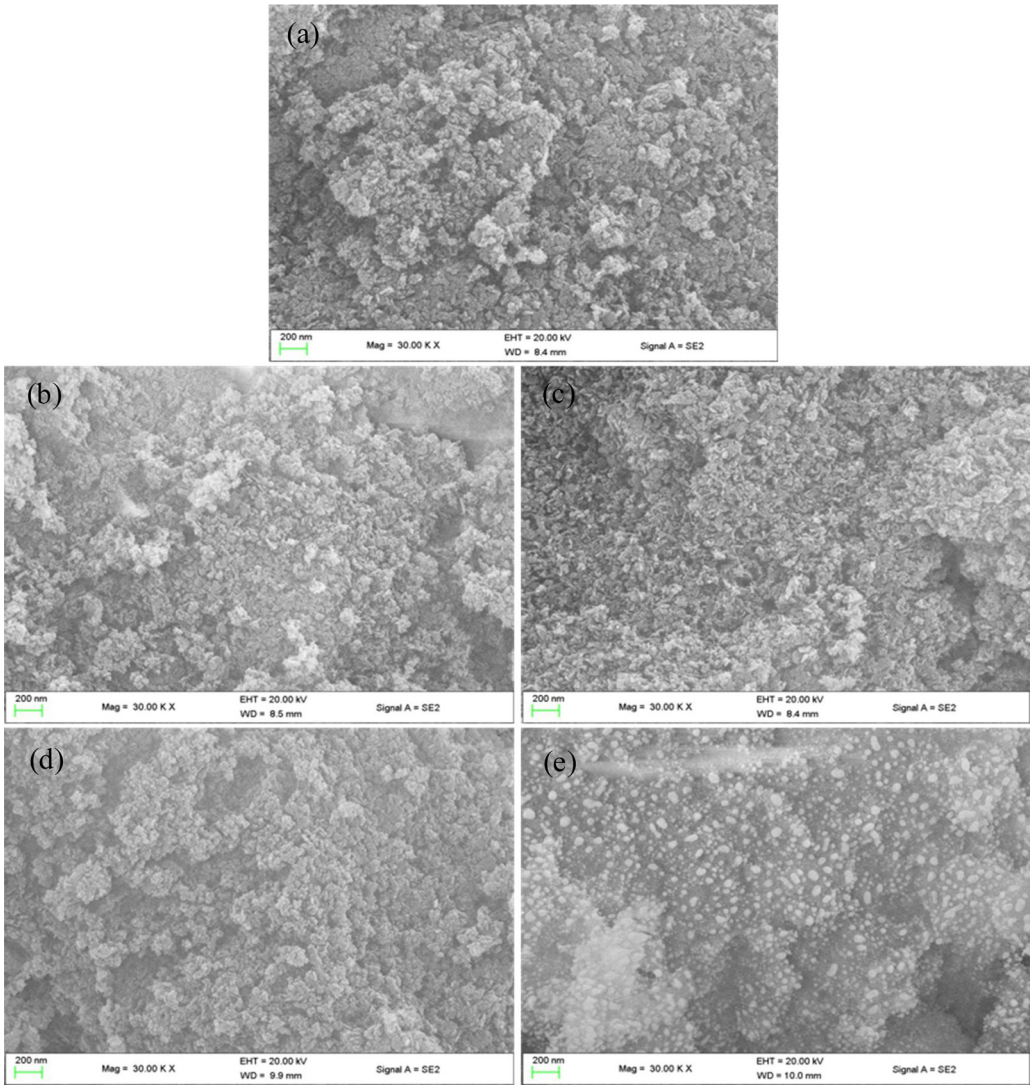

Fig. 3. SEM images of (a) γ-Al_2O_3 support, (b) 2.5 % Mn/γ-Al_2O_3, (c) 5 % Mn/γ-Al_2O_3, (d) 7.5 % Mn/γ-Al_2O_3; and (e) 10 % Mn/γ-Al_2O_3 catalysts.

loaded on γ-Al_2O_3 catalysts.

Table 4 shows the BET results for pure SiO_2 support, 2.5 % Mn/SiO_2 and 7.5 % Mn/SiO_2 catalysts. The BET surface area of pure SiO_2 support was found to be 506.0 m^2/g. However, the surface area of SiO_2 anticipated to decrease with Mn loadings and it was observed that when 2.5 wt% Mn was loaded on SiO_2, the surface area was found to be 339.6 m^2/g which further decreased to 279.9 m^2/g upon 7.5 wt% of Mn loading. We can observe from the Table 4 that BET surface area and pore volume were decreased with the increase in the Mn metal loading from 2.5 to 7.5 wt%. The decrease in surface area and pore volume can be attributed to the tendency of metal particles to form aggregates leaving the measurable internal volume as pores.

The surface area analysis was done to relate the surface areas of the catalysts to the percentage conversion and selectivities in the ozonation of 1,2-dichlorobenzene. The catalysts with the higher surface area showed an effect in its activity in the ozone initiated oxidation of 1,2-dichlorobenzene, showing the higher conversions and selectivities towards the main products.

3.2. Characterisation of ozonation reaction product

3.2.1. Fourier transform-infrared spectroscopy (FT-IR)

Fig. 7 display the FT-IR spectrum for the main product (mucochloric acid), the spectrum shows adsorption band at 1598 cm^{-1} which is assigned to C═O functional group. The C–H stretching is observed at 878 cm^{-1} and 1250 cm^{-1}. The OH vibrational stretching appeared at 3498 cm^{-1}. Functional groups that are observed in the IR spectrum tend to be in good agreement with spectrum corresponding to mucochloric acid.

3.2.2. Gas chromatography– mass spectroscopy

The identification of the reaction products mixture was done by gas chromatography which was coupled with mass spectrometry detector in order to facilitate the identification of compounds that are in the reaction mixture by elucidation of the molar mass. Fig. 8(a) show the chromatogram of 1,2-dichlorobenzene before ozonation, while Fig. 8(b) show the chromatogram of 1,2-dichlorobenzene after 24 h of ozonation. The peak at retention time 17.8 min refers to mucochloric acid which was identified as the main product of ozonation of 1,2-dichlorobenzene. The peak at retention time 8.4 min and 8.2 min are attributed to 1,2-dichlorobenzene (un-reacted) and 3,4-dichloro-2,5-furadione respectively. Scheme 1 represents the oxidation products formed from the ozonation of 1,2-dichlorobenzene.

Fig. S7 shows the mass spectra of (a) 1,2-dichlorobenzene (b) 3,4-dichloro-2,5-furandione and (c) mucochloric acid. The base peak at m/z = 168 represent the $M^{+\cdot}$ of mucochloric acid, while the base peak at m/z = 133 represent the fragments due to the cleavage of one Cl^- ion. The series of ions are detected at m/z = 87, m/z = 29 and m/z = 60 is

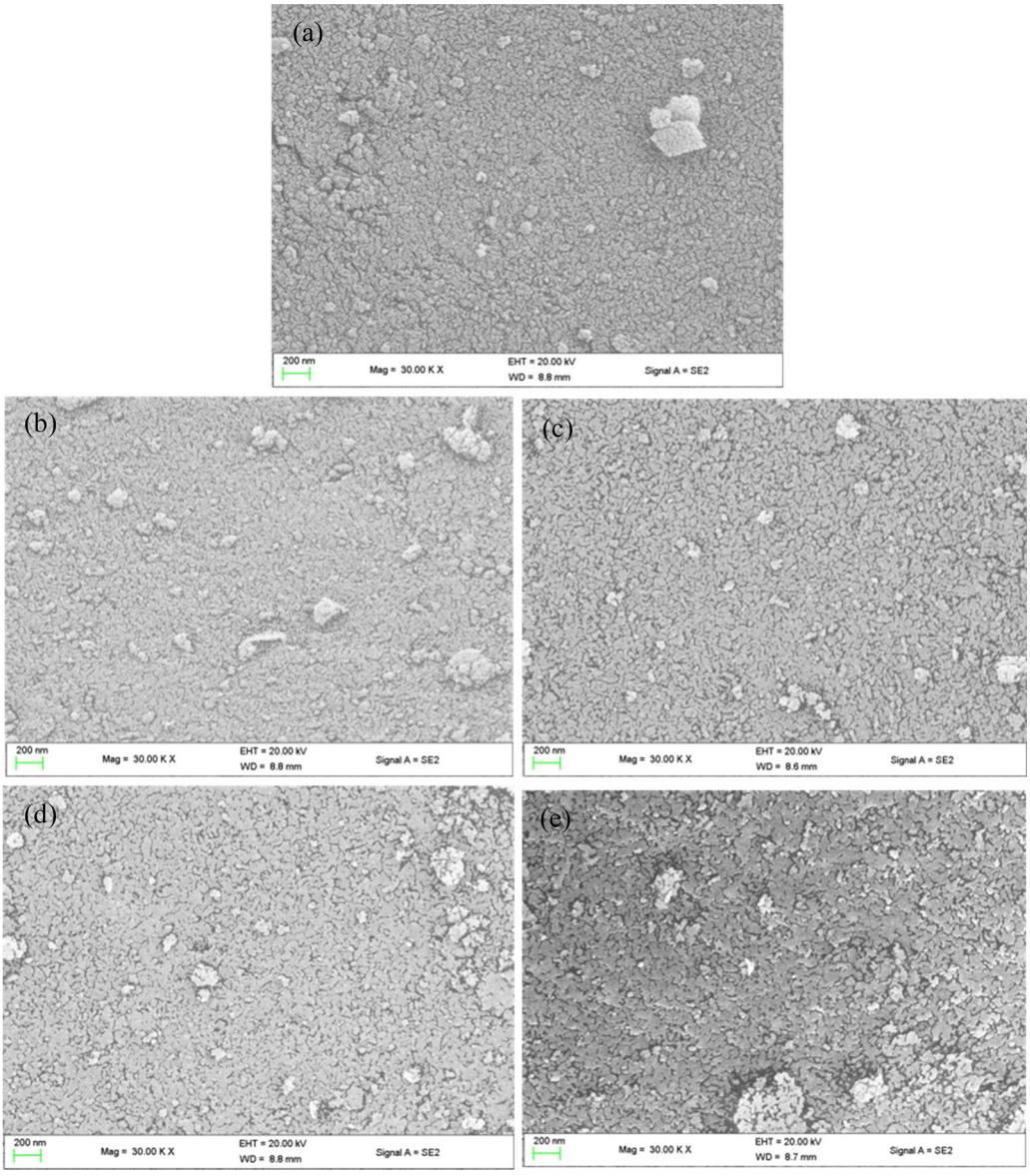

Fig. 4. SEM images of (a) SiO_2 support, (b) 2.5 % Mn/SiO_2, (c) 5 % Mn/SiO_2, (d) 7.5 % Mn/SiO_2 and (e) 10 % Mn/SiO_2 catalysts.

due radicals O = C-C(Cl)-C, C − OH and CH-C(Cl) respectively. In the mass spectrum of 3,4-dichloro-2,5-furandione, the molecular ion of $m/z = 166$ represents of $M^{+\cdot}$ of 3,4-dichloro-2,5-furandione. The series of base peaks at $m/z = 122$, $m/z = 87$, and $m/z = 59$ which represent M^+ fragments of 3,4-dichloro-2,5-furandione are due to radicals C(Cl) =C(Cl)C = O, O = C-C(Cl)-C and C-O respectively.

The presence of unreacted 1,2-dichlorobenzene was confirmed by comparing Fig. 8(a) and (b) which shows the retention time of 1,2-dichlorobenzene to be 8.4 min. The calculation of conversion and percentage selectivity was done by using the gas chromatogram. The percentage conversion was calculated on peak area of substrate out of total peak area in the chromatogram, while the selectivity was expressed as amount of individual product formed out of total amount of substrate converted as percentage. The undefined products were formed due to further oxidation of initial product into simpler compounds that are said to be less toxic and more biodegradable.

3.3. Oxidation of 1,2-dichlorobenzene

3.3.1. Percentage conversion

Tables S5–S12 display the catalytic performance of $Mn/\gamma\text{-}Al_2O_3$ and Mn/SiO_2 catalysts in terms of percentage conversion in the ozonation reactions of 1,2-dichlorobenzene. Reaction samples were drawn after 3, 6, 9, 12, 15, 18 and 24 h of ozonation time at ambient reaction conditions. Blank ozonation, $\gamma\text{-}Al_2O_3$ and SiO_2 catalyzed ozonation reaction were initially done. The comparative results on the activity based on percentage conversion of uncatalyzed, activated charcoal, pure $\gamma\text{-}Al_2O_3$, pure SiO_2, various Mn loaded $\gamma\text{-}Al_2O_3$, and various Mn loaded SiO_2 catalysts are shown in Fig. 9. It can be seen from Tables S1–S4, the ozonation reactions that were performed in the absence of catalyst and in the presence of supports only (pure $\gamma\text{-}Al_2O_3$ and SiO_2) show low percentage conversions after 24 h ozonation reaction (25 %, 30 % and 31 % respectively).

Literature shows that activated charcoal (AC) can be a promising alternative to the treatment of wastewaters which contains organic contaminants. It is believed that AC promotes aqueous ozone decomposition leading to the formation of active species, which are oxygenated. The oxygenated species are responsible for enhancing organic compounds oxidation/mineralization, making activated charcoal a promising candidate in the ozonation reactions [33]. In the activated charcoal catalyzed ozonation reaction, the selectivity towards mucochloric acid found as decreasing with increased ozonation time from 9

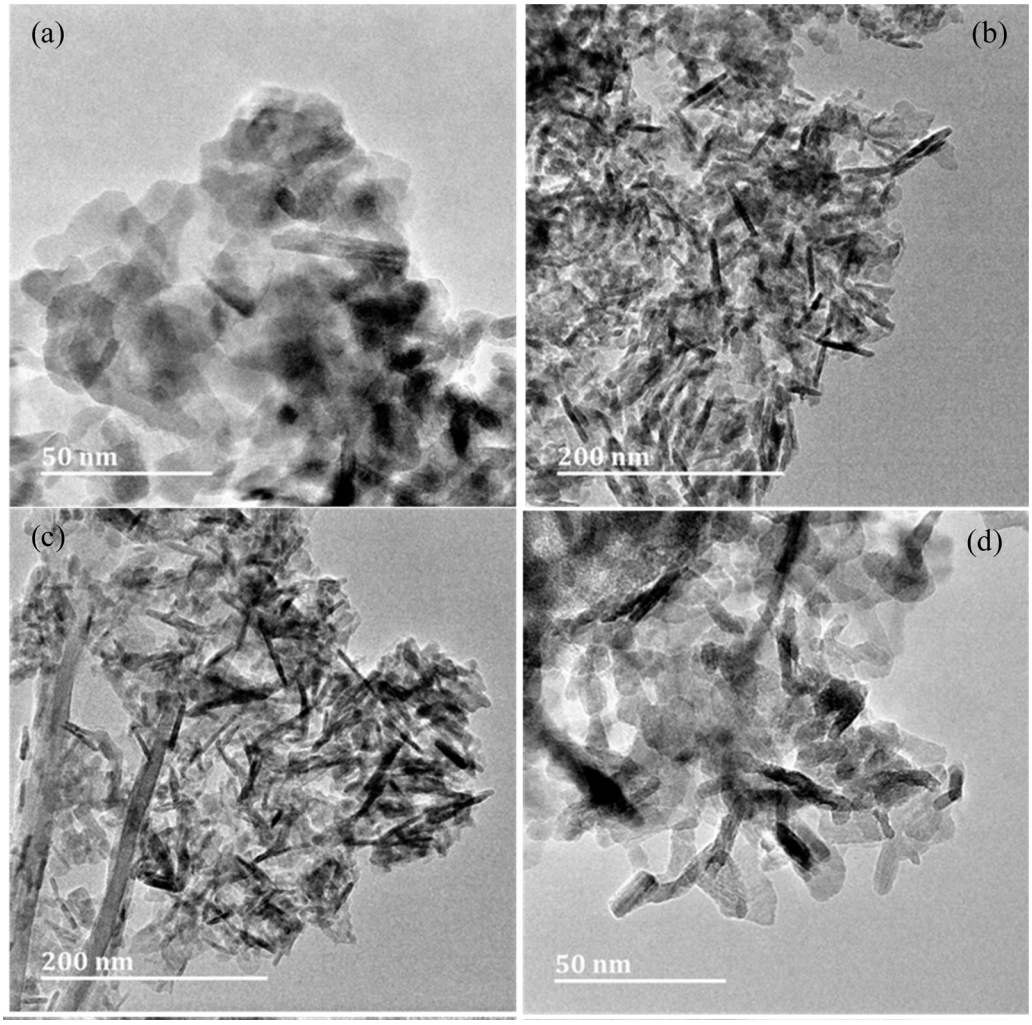

Fig. 5. TEM images of (a) γ-Al_2O_3 support, (b) 2.5 % Mn/γ-Al_2O_3, (c) 5 % Mn/γ-Al_2O_3, and (d) 7.5 % Mn/γ-Al_2O_3 catalysts.

to 24 h (Table S2). While in 5 % Mn/SiO_2 catalyzed ozonation reaction, the selectivity towards mucochloric acid was observed as increasing with increased ozonation time from 3 to 24 h (Table S10). The ozonation reaction catalyzed by 5 % Mn/SiO_2 showed high percentage conversion (44 %) towards the oxidation of 1,2-dichlorobenzene after 24 h than ozonation reactions performed with the uncatalyzed, activated charcoal, pure γ-Al_2O_3, pure SiO_2, 2.5 %, 7.5 %, 10 %Mn/γ-Al_2O_3, 2.5 %, 7.5 %, 10 % Mn/SiO_2 catalyzed reactions, followed by 5 % Mn/γ-Al_2O_3 catalyzed reactions (Tables S1–S12).

From the Tables S1–S4, it can be observed that in the ozone initiated oxidation of 1,2-dichlorobenzene results in the formation of the 3,4-dichloro-2,5-furandione and mucochloric acid as products. In the uncatalysed, activated charcoal, γ-Al_2O_3 and SiO_2 catalysed reactions there is no correlation or control over the product formation in terms of conversion and selectivities (Tables S1–S4). Mn loaded γ-Al_2O_3 catalysts resulted in the low concentration of mucochloric acid at the initial stages and the concentration of the 3,4-dichloro-2,5-furandione was higher (Tables S5–S8). Upon the increased reaction time the concentration of 3,4-dichloro-2,5-furandione was decreased and concentration of mucochloric acid was increased. In these reactions the unidentified products only formed after 12 h of ozonation, this also suggests that the 1,2-dichlorobenzene results in the initial formation of 3,4-dichloro-2,5-furandione and this further gets oxidized to produce mucochloric acid as the main product.

Mn loaded SiO_2 resulted in only the 3,4-dichloro-2,5-furandione and mucochloric acid as products. Whereas, Mn loaded γ-Al_2O_3 yielded unidentified products in addition to the 3,4-dichloro-2,5-furandione and mucochloric acid (Tables S9–S12). The results from these tables clearly indicating that in the ozonation of 1,2-dichlorobenzene, ozone interacts with substrate and forms 3,4-dichloro-2,5-furandione as the product. 3,4-Dichloro-2,5-furandione product upon further reaction with ozone produces mucochloric acid.

3.3.2. Percentage selectivity

Initially 5 % Mn/SiO_2 calcined catalyst resulted in the highest selectivity towards mucochloric acid (62 %) and during 12 h of ozonation 5 % Mn/SiO_2 and 5 % Mn/γ-Al_2O_3 catalysts resulted in the highest selectivity of 72 and 73 % respectively as shown in Fig. 10(a). During the 18 h of ozonation γ-Al_2O_3 support catalyst showed the lowest selectivity (50 %) towards mucochloric acid. After 24 h of ozonation 5 % Mn/SiO_2 and 5 % Mn/γ-Al_2O_3 calcined catalysts showed a better selectivity towards mucochloric acid (88 % and 86 % respectively). The results show highest selectivity with 5 % Mn/SiO_2, possibly due to more surface area available for the selective oxidation of mucochloric acid. Fig. 10(b) showed that as the ozonation time increases the selectivity towards 3,4-dichloro-2,5-furandione decreases in the oxidation of 1,2-dichlorobenzene (Tables S5–S12), suggesting the further oxidation of 3,4-dichloro-2,5-furandione to mucochloric acid.

4. Conclusions

The selective oxidation of 1,2-dichlobenzene has been challenging

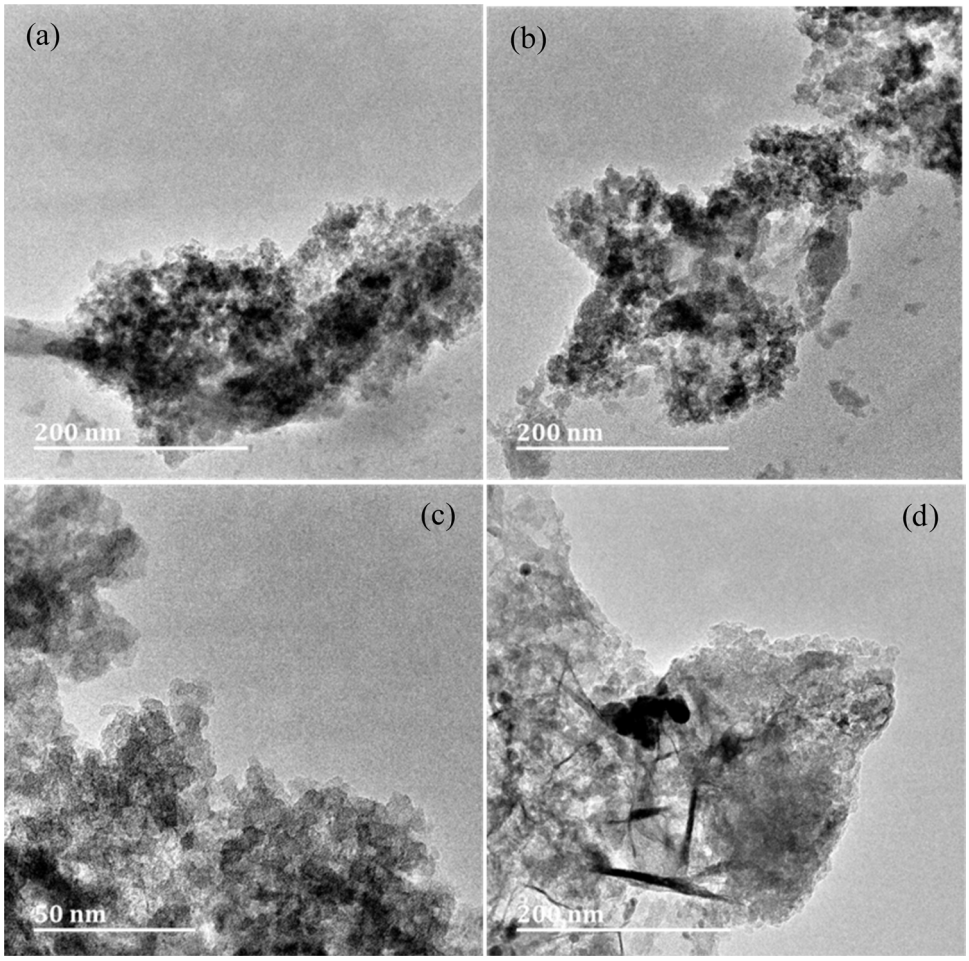

Fig. 6. TEM images for a) SiO_2 b) 2.5 % Mn/SiO_2 and c) 5 % Mn/ SiO_2 and (d) 7.5 % Mn/ SiO_2 catalysts.

Table 1
Manganese wt% on each $Mn/\gamma\text{-}Al_2O_3$ catalyst analyzed using ICP-OES and EDX.

	Theoretical Mn wt%	ICP Mn wt%	EDX Mn wt%
2.5 % $Mn/\gamma\text{-}Al_2O_3$	2.50	1.95	1.47
5.0 % $Mn/\gamma\text{-}Al_2O_3$	5.00	6.46	4.08
7.5 % $Mn/\gamma\text{-}Al_2O_3$	7.50	2.48	5.60
10 % $Mn/\gamma\text{-}Al_2O_3$	10.0	4.26	11.93

Table 2
Manganese wt% on each Mn/SiO_2 catalyst analyzed using ICP-OES and EDX.

Catalyst	Theoretical Mn wt%	ICP Mn wt%	EDX Mn wt%
2.5 % Mn/SiO_2	2.50	0.33	2.12
5.0 % Mn/SiO_2	5.00	1.75	5.10
7.5 % Mn/SiO_2	7.50	2.63	8.17
10.0 % Mn/SiO_2	10.0	3.44	19.83

Table 3
BET surface areas for the various Mn loaded $\gamma\text{-}Al_2O_3$ catalysts.

Catalyst sample	BET Surface Area (m^2/g)	Pore Volume (cm^3/g)	Pore Size (nm)
Pure $\gamma\text{-}Al_2O_3$	**295.0**	–	–
2.5 % $Mn/\gamma\text{-}Al_2O_3$	167.6	0.3826	9.13
7.5 % $Mn/\gamma\text{-}Al_2O_3$	107.8	0.3022	11.21

Table 4
BET surface areas for the various Mn loaded SiO_2 catalysts.

Catalyst sample	BET Surface Area (m^2/g)	Pore Volume (cm^3/g)	Pore Size (nm)
Pure SiO_2	**506.0**	–	–
2.5 % Mn/SiO_2	339.6	0.009591	7.28
7.5 %Mn/SiO_2	279.9	0.007381	8.24

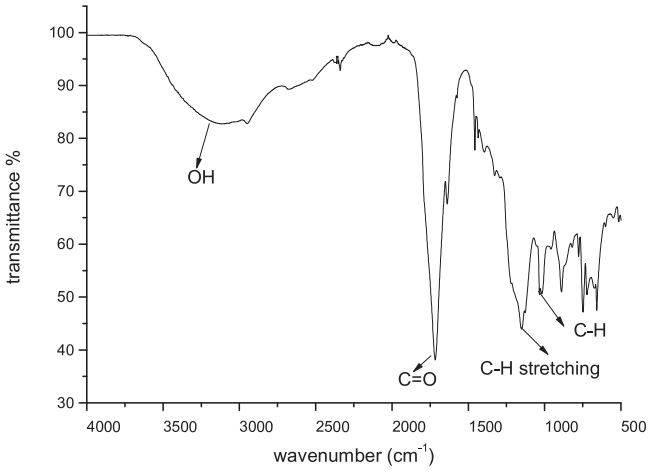

Fig. 7. FT-IR spectrum of reaction product mucochloric acid.

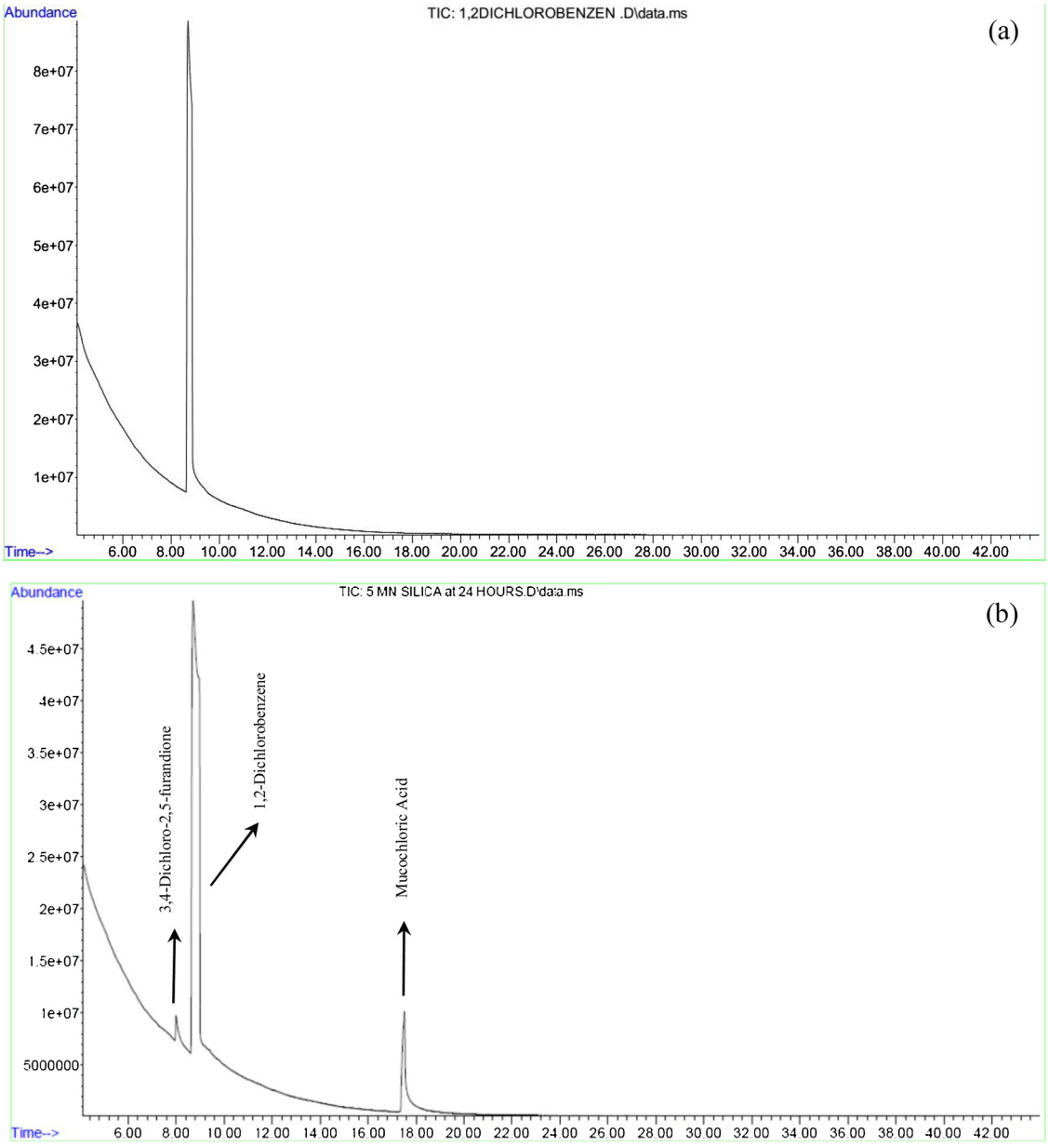

Fig. 8. Gas chromatograms of 1,2-dichlorobenzene a) before ozonation and b) after 24 h of ozonation using 5 % Mn/SiO_2 catalyst.

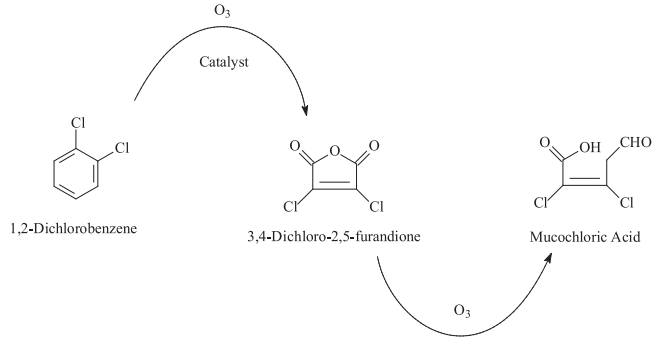

Scheme 1. Oxidation products formed from the ozonation of 1,2-dichlorobenzene.

due to the non-biodegradable nature and high resistance of the chlorinated aromatic compounds towards chemical oxidation. The studies have been conducted with a wide range of catalytic systems so as to identify the most suitable catalytic system for efficient oxidation of chlorinated aromatics into biodegradable and less toxic organics at ambient reaction conditions. The ozone initiated catalytic oxidation of 1,2-dichlorobenzene at ambient temperature and pressure conditions was investigated. The main product mucochloric acid and the minor product 3,4-dichloro-2,5-furandione were positively identified in the 24 h ozonation reaction. All the catalysts including activated charcoal resulted in the similar ozonation products as it is observed in un-catalyzed ozonation reaction. Bare γ-Al_2O_3 and SiO_2 nano catalysts were found to be active in the catalytic oxidation of 1,2-dichlorobenzene with moderate percentage selectivity toward formation of mucochloric acid. The manganese doped γ-Al_2O_3 catalysts and also manganese doped SiO_2 catalysts exhibited high activity in the conversion of 1,2-dichlorobenzene with high selectivity towards mucochloric acid compared to that of bare γ-Al_2O_3 and SiO_2 powder. This shows that manganese acts as active site on the surface and within the pores of gamma alumina and silica supports. The 5 % Mn/SiO_2 catalyst was found to be the most active catalyst towards the main product with respect to % conversion (44 %) and also it was found to be the most

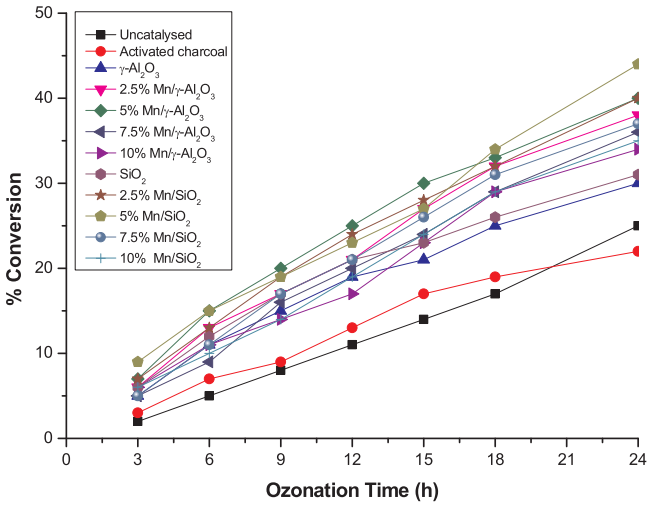

Fig. 9. Percentage conversions with uncatalyzed, activated charcoal, pure γ-Al_2O_3, various Mn loaded γ-Al_2O_3 catalysts, pure SiO_2 and various Mn loaded SiO_2 catalysts.

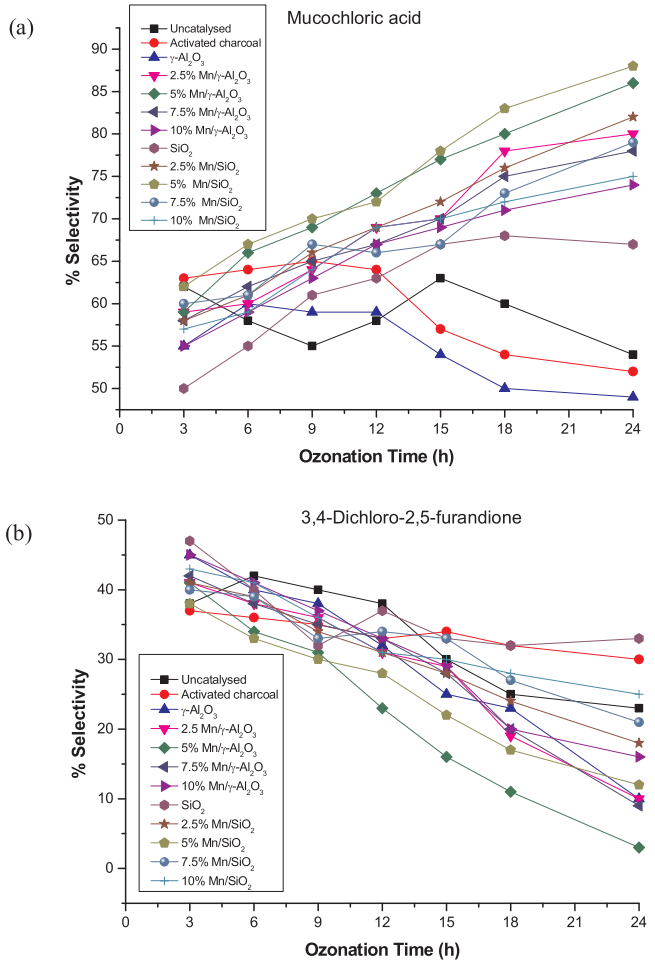

Fig. 10. Percentage selectivity towards (a) Mucochloric acid and (b) 3,4-Dichloro-2,5-furandione with uncatalyzed, activated charcoal, pure γ-Al_2O_3, various Mn loaded γ-Al_2O_3 catalysts, pure SiO_2 and various Mn loaded SiO_2 catalysts.

selective catalyst towards the main product % selectivity (88 %). This study illustrated on how the surface area and pore volumes of the employed catalysts played a critical role in the oxidation of 1,2-dichlorobenzene. The catalysts with the higher surface area displayed their catalytic activity by showing the higher conversions and selectivities towards the main products. This study also revealed that the activity of the catalysts in the catalytic ozonation of 1,2-dichlorobenzene is affected (lead to poor activity) by the increase in manganese loading greater than 5 %.

CRediT authorship contribution statement

Nomthandazo Mkhize: Formal analysis, Investigation, Writing - original draft. **Prabal Pratap Singh:** Formal analysis. **Deepak Kumar Das:** Formal analysis. **Viswanadha Srirama Rajasekhar Pullabhotla:** Conceptualization, Supervision, Methodology, Formal analysis, Writing - original draft, Writing - review & editing, Funding acquisition.

Declaration of Competing Interest

The authors declare no conflict of interest.

Acknowledgments

The authors acknowledge the EMU at the University of KwaZulu-Natal, Westville campus, for providing us access to their TEM facility. Rajasekhar Pullabhotla would like to acknowledge the Research and Innovation Office, UZ, for the financial support in the form of Project S 451/12 and the National Research Foundation (NRF, South Africa) for the financial support in the form of the Incentive Fund Grant (Grant No: 103691) and Research Developmental Grant for Rated Researchers (112145).

Appendix A. Supplementary data

Supplementary material related to this article can be found, in the online version, at doi:https://doi.org/10.1016/j.cattod.2020.06.025.

References

[1] J. Levec, A. Pintar, Catalytic oxidation of aqueous solutions of organics. An effective method for removal of toxic pollutants from waste waters, Catal. Today 24 (1995) 51–58.
[2] M.L. Hitchman, R.A. Spackman, N.C. Ross, C. Agra, Disposal methods for chlorinated aromatic waste, Chem. Soc. Rev. 24 (6) (1995) 423–430.
[3] Sang Chai Kim, The catalytic oxidation of aromatic hydrocarbons over supported metal oxide, J. Hazard. Mater. B 91 (2002) 285–299.
[4] M. Tiana, C. Hea, Y. Yua, H. Panc, L. Smith, Z. Jianga, N. Gaoa, Y. Jiana, Z. Haod, Q. Zhua, Catalytic oxidation of 1,2-dichloroethane over three-dimensional ordered meso-macroporous Co_3O_4/La0.7Sr0.3Fe0.5Co0. $5O_3$: destruction route and mechanism, Appl. Catal.: Gen. 553 (2018) 1–14.
[5] E. Pelizzet, M. Borgarrello, E. Borgarrello, N. Serpone, Photocatalytic degradation of polychlorinated dioxins and polychlorinated biphenyls in aqueous suspensions of semiconductors irradiated with simulated solar light, Chemosphere 17 (3) (1988) 499–510.
[6] S. Krishnamoorthy, Juan A. Rivas, Michael D. Amiridis, Catalytic oxidation of 1,2-dichlorobenzene over supported transition metal oxides, J. Catal. 193 (2000) 264–272.
[7] R. Weber, T. Sakurai, H. Hagenmaier, Low temperature decomposition of PCDD/PCDF, chlorobenzenes and PAHs by TiO_2-based V_2O_5 –WO_3 catalysts, Appl. Catal. B: Environ. 20 (1999) 249–256.
[8] E.C. Chetty, V.B. Dasireddy, Suresh Maddila, S.B. Jonnalagadda, Efficient conversion of 1,2-dichlorobenzene to mucochloric acid with ozonation catalyzed by V_2O_5 loaded metal oxides, Appl. Catal. B Environ. 117 (2012) 18–28.
[9] R. Andreozzi, A. Insola, V. Caprio, R. Marotta, V. Tufano, The use of manganese dioxide as a heterogeneous catalyst for oxalic acid ozonation in aqueous solution, Appl. Catal. A Gen. 138 (1996) 75–81.
[10] P.S. Ghuge, K.A. Saroha, Catalytic ozonation for the treatment of synthetic and industrial effluents- Application of mesoporous material: a review, J. Environ. Manage. 211 (2018) 83–102.
[11] X. Li, W. Chen, L. Ma, H. Wang, J. Fan, Industrial wastewater advanced treatment via catalytic ozonation with an Fe-based catalyst, Chemosphere 195 (2018) 336–343.
[12] E. Gilbert, Biodegradability of ozonation products as a function of COD and DOC elimination by the example of humic acids, Water Res. 22 (1) (1988) 123–126.
[13] S. Tong, W. Liu, W. Leng, Q. Zhang, Characteristics of MnO_2 catalytic ozonation of sulfosalicylic acid and propionic acid in water, Chemosphere 50 (2003) 1359–1364.

[14] B. Kassprzyk-Hordern, M. Ziolek, J. Nawrocki, Catalytic ozonation and methods of enhancing ozone reactions in water treatment, Appl. Catal. B Environ. 46 (2003) 639–669.
[15] J. Nawrocki, B. Kassprzyk-Hordern, The efficiency and mechanisms of catalytic ozonation, Appl. Catal. B Environ. 99 (2010) 27–42.
[16] J.H. Larsen, M. Lee, P.C. Frost, G.A. Lamberti, D.M. Lodge, Variable toxicity of ionic liquid–forming chemicals to Lemna mino and the influence of dissolved organic matter, Environ. Toxical. Chem. 27 (3) (2008) 676–681.
[17] C. Cooper, R. Burch, An investigation of catalytic ozonation for the oxidation of halocarbons in drinking water preparation, Water Res. 33 (18) (1999) 3695–3700, https://doi.org/10.1016/S0043-1354(99)00091-3.
[18] M.A. Banares, Supported metal oxide and other catalysts for ethane conversion: a review, Catal. Today 51 (1999) 319–348.
[19] C.A. Orgea, J.J.M. Órfão, M.F.R. Pereira, A.M.D. de Farias, R.C.R. Neto, M.A. Fraga, Ozonation of model organic compounds catalysed by nanostructured cerium oxides, Appl. Catal. B Environ. 103 (2011) 190–199.
[20] W. Deng, Q. Dai, Y. Lao, B. Shi, X. Wang, Low temperature catalytic combustion of 1,2-dichlorobenzene over CeO_2-TiO_2 mixed oxide catalysts, Appl. Catal. B Environ. 181 (2016) 848–861.
[21] J. Ma, N.J.D. Graham, Preliminary investigation of manganese-catalyzed ozonation for the destruction of atrazine, Ozone Sci. Eng. 19 (1997) 227–240.
[22] S.T. Oyama, Chemical and catalytic properties of ozone, Catal. Rev.: Sci. Eng. 42 (2000) 279–322.
[23] X. Chen, J. Jiang, F. Yan, S. Tiana, K. Lia, A novel low temperature vapor phase hydrolysis method for the production of nano-structured silica materials using silicon tetrachloride, RSC Adv. 4 (2014) 8703.
[24] V.S.R.R. Pullabhotla, A. Rahman, S.B. Jonnalagadda, Selective catalytic knoevenagel condensation by Ni-SiO_2 supported heterogeneous catalysts: an environmental benign approach, Catal. Commun. 10 (2009) 365–369.
[25] S. Banerjee, S. Dubey, R.K. Gautam, M.C. Chattopadhyaya, Y.C. Sharma, Adsorption characteristics of alumina nanoparticles for the removal of hazardous dye, Orange G from aqueous solutions, Arab. J. Chem. 12 (8) (2017) 5339–5354 2019.
[26] H. Xia, Y. Wan, F. Yan, L. Lu, Manganese oxide thin films prepared by pulsed laser deposition for thin film microbatteries, Mater. Chem. Phys. 143 (2014) 720–727.
[27] R. Nandanwar, P. Singh, F.Z. Haque, Synthesis and characterization of SiO_2 nanoparticles by sol-gel process and its degradation of methylene blue, Am. Chem. Sci. J. 5 (2015) 1–10.
[28] S. Musić1, N. Filipović-Vinceković, L. Sekovanić, Precipitation of amorphous SiO_2 particles and their properties, Braz. J. Chem. Eng. 28 (01) (2011) 89–94.
[29] A.A. Tyganenko, P.P. Mardilovich, Structure of alumina surfaces, Faraday Trans. 92 (23) (1996) 4843–4852.
[30] C.J. Lucio-Ortiz, J.R. De la Rosa, A.H. Ramirez, J.A. De los Reyes Heredia, P. Del Angel, S. Munoz-Aguirre, L.M. De Leon-Covian, Synthesis and characterization of Fe doped mesoporous Al_2O_3 by sol-gel method and its use in trichloroethylene combustion, J. Solgel Sci. Technol. 58 (2011) 374–384.
[31] K. Panwar, M. Jassal, A.K. Agrawal, In situ synthesis of Ag-SiO_2 Janus particles with epoxy functionality for textile applications, Particuology 19 (2015) 107–112.
[32] Y. Cui, X. Bu, H. Zou, X. Xu, D. Zhou, H. Liu, H. Sun, J. Jiang, H. Zhang, A dual solvent evaporation route for preserving carbon nanoparticle fluorescence in silica gel and producing white light-emitting diodes, Mater. Chem. Front. 1 (2017) 387–393.
[33] P.C.C. Faria, J.J.M. Orfao, M.F.R. Pereira, Activated carbon catalytic ozonation of oxamic and oxalic acids, Appl. Catal. B Environ. 79 (2008) 237–243.